ELSEVIER

Journal of Alloys and Compounds 281 (1998) 290–300

Journal of ALLOYS AND COMPOUNDS

The investigation of the $Zr_{1-y}Ti_y(Cr_{1-x}Ni_x)_2$–$H_2$ system $0.0 \leq y \leq 1.0$ and $0.0 \leq x \leq 1.0$ Phase composition analysis and thermodynamic properties

M. Bououdina[1,*], H. Enoki, E. Akiba

National Institute of Materials and Chemical Research, 1-1 Higashi, Tsukuba, Ibaraki 305, Japan

Received 17 June 1998; received in revised form 29 July 1998

Abstract

The $Zr_{1-y}Ti_y(Cr_{1-x}Ni_x)_2$ compounds were synthesized and characterized by means of X-ray powder diffraction. From the Rietveld analysis carried out on the alloys, we determined the phase abundancy and refined the crystal structure. The system crystallized with hexagonal C14-type structure for nickel content less than $x=1.0$ with some amount of additional phases (ZrNi, Zr_9Ni_{11}, Zr_7Ni_{10}, TiNi) and pure metals (Ni and Cr). For higher nickel concentrations, the system crystallized in the cubic C15-type structure. The amount of additional phases increased with increasing nickel and titanium content. The Pressure–Composition–Temperature measurements using a volumetric method were carried out at 313 K on some selected alloys. The single phase systems were found to absorb a large amount of hydrogen ($H/M \leq 1.8$ wt.%) but had very poor kinetics. The multiphase systems were found to behave as a single phase (presence of single plateau), have a relatively good hydrogen capacity ($H/M \leq 1.4$ wt.%) and exhibit faster kinetics. A linear correlation between the heat of formation of the $Zr_{1-y}Ti_y(Cr_{1-x}Ni_x)_2$ hydrides estimated from the band structure model and the unit cell volume of the alloys determined from the X-ray Rietveld analysis was obtained. It shows a decrease of hydride stability with increasing unit cell volume.

Keywords: Laves phases; Multiphase system; Hydrogen in metals; Kinetics

1. Introduction

The Zr-based Laves phases have been studied extensively as potential hydrogen storage materials and in particular as a negative electrode for Ni–MH batteries. The $ZrCr_2$ prototype crystallizes either in the hexagonal C14-type and the cubic C15-type structures. The corresponding hydride absorbs about 3.4 H/f.u.. Nevertheless, it was not proposed for such technological application due to the strong stability of its hydride at room temperature (the equilibrium pressure at 293 K is 12 kPa [1,2]). Many studies have been devoted to the substitution of the two elements by other transition metals in order to modify the hydriding properties.

It is well known that the $ZrNi_2$ compound does not exist [3]. Nevertheless, replacement of Cr in $ZrCr_2$ by Ni is possible. The Ni substitution has been shown to increase the plateau pressure and to conserve a large hydrogen capacity in comparison to substitutions of elements less attractive than Cr (M=Co and Fe [2], Cu [4], Si and Ge [5], Al [6]). In their study of the $Zr(Cr_{1-x}Ni_x)_2$ system, Blazina et al. [7] found that the replacement of some amount of Cr by Ni (up to 50%), made the system crystallize in the hexagonal structure and increased the plateau pressure, but the hydride was still stable at room temperature. In our crystal structure studies by neutron diffraction of the $Zr(Cr_{1-x}Ni_x)_2$ system with $0.0 \leq x \leq 0.4$ [8,9], we found that the system is multiphase, for all compositions other than $x=0$. For $x \neq 0$, the system contained additional phases (ZrNi, Zr_9Ni_{11}) and some amount of pure metals (Cr, Ni). In a recent article published by Joubert et al. [10] on the system Zr–Cr–Ni, it was found that the samples are multiphase. The P–C–T diagrams measured at 298 K on some selected samples showed an increase of the plateau pressure with decreasing hydrogen capacity but the corresponding hydrides can not be completely dehydrogenated. In their neutron diffraction study of the $ZrCr_{1.2}Ni_{0.8}D_{3.3}$, the previous authors [11] found that after 1 month of annealing at 1273 K the corresponding alloy still contained extra phases (about 3% of ZrNi and 2% of pure Cr).

Most efforts on the $ZrCr_2$ Laves phases were put into increasing its plateau pressure by substitution into the

*Corresponding author.

[1]a: STA fellow

0925-8388/98/$ – see front matter
PII: S0925-8388(98)00792-0

Cr-site. Hitherto, no systematic study of a quaternary system based on the $ZrCr_2$ compound from the point of view of phase analysis and crystal structure has been done. For this purpose, we were interested in investigating the $Zr_{1-y}Ti_y(Cr_{1-x}Ni_x)_2$ system.

In the AB_2 type compounds, the change of the metallic A-site size (Zr by Ti) is about three times larger than that of the B-site (Cr by Ni), $[(r_{Zr}-r_{Ti})/(r_{Zr})]=8.7\%$ and $[(r_{Cr}-r_{Ni})/(r_{Cr})]=2.8\%$. The susbtitution of Ni for Cr will have a smaller effect on the increase of the plateau pressure as it has been found in previous works [7]. It was found also, that for higher nickel contents ($x_{Ni}>0.5$), a secondary phase Zr_7Ni_{10} appeared and its amount increased with the increasing Ni content [10]. The Zr_7Ni_{10} phase has a lower plateau pressure ($P_{eq}=0.04$ bars at $T=298$ K [24,25]), so its presence will reduce the hydrogen capacity. In our previous studies [8,9], we found that the replacement of some amount of Cr by Ni ($x_{Ni}\leq 0.4$) has almost no effect on the hydrogen capacity. On the other hand, the replacement of Zr by Ti will increase the plateau pressure and contribute to the increase of the hydrogen capacity in weight percentage.

From our systematic study of the $Zr_{1-y}Ti_y(Cr_{1-x}Ni_x)_2$–$H_2$ system, we expect a better control of the plateau pressure by the modification of the Zr/Ti and Cr/Ni ratios and to reach a higher hydrogen capacity. A map of relationships phase of the pseudo-binary $Zr_{1-y}Ti_y(Cr_{1-x}Ni_x)_2$ ($0.0\leq y\leq 1.0$ and $0.0\leq x\leq 1.0$) system will be established.

In this article, we present the quantitative phase analysis of the $Zr_{1-y}Ti_y(Cr_{1-x}Ni_x)_2$ alloys determined by means of the Rietveld method and the evolution of the lattice parameters with Ti and Ni contents. The hydriding properties of the system were characterised using the P–C–T diagrams measured on selected samples.

2. Experimental details

Eighteen samples of the $Zr_{1-y}Ti_y(Cr_{1-x}Ni_x)_2$ ($0.0\leq y\leq 1.0$ and $0.0\leq x\leq 1.0$) series were prepared using the arc melting technique under highly pure argon. The pure elements with relatively high purity (99.9) were put in the crucible. After repeated argon filling and evacuation, about 0.9 atm of Ar pressure was admitted into the system. The samples were then melted several times (4–5) to ensure a good homogeneity.

All samples were characterised using X-ray powder diffraction. The measurement were performed on a Rigaku RAX-I diffractometer with Cu Kα radiation. The structural refinements were carried out using the Rietveld method. We used the RIETAN-97 beta version software developed by Izumi [12].

The P–C–T measurements done on selected samples were carried out using a conventional volumetric system [13]. The samples were crushed into powder using a stainless steel mortar and then introduced into a container. The activation process was achieved by performing three heating–cooling cycles: after evacuating the system using a rotary pump ($P=10^{-3}$ atm) and then a diffusion pump ($P<10^{-5}$ atm) for 1 h, about 50 bar of hydrogen was admitted into the reactor, then the system was heated to 573 K for 1 h. Subsequently, the system was cooled down to room temperature. Before the PCT measurements, the samples were heated up to 573 K under high vacuum for 1–3 h to ensure a complete desorption.

3. Results and discussion

3.1. Crystal structure and phases abundancy

The as-cast alloys of the $Zr_{1-y}Ti_y(Cr_{1-x}Ni_x)_2$ series with $0.0\leq x_{Ni}\leq 0.5$ crystallized in the hexagonal C14-type structure. For $x_{Ni}>1.0$, the system crystallized in the cubic C15-type structure. The measured X-ray powder diffraction patterns showed a few extra peaks from additional phases.

The C36-type hexagonal phase ($c_{C36}=2\times c_{C14}$) was observed in the X-ray diffraction patterns of the binary alloys $ZrCr_2$ and $TiCr_2$. The C36-type can easily be distinguish from the C14-type by the Rietveld method. From the Rietveld quantitative phase analysis, we found about 47% of C36 in both alloys.

The BCC structure $Ti_{1-x}Cr_x$ [15] was also observed in the X-ray diffraction patterns. The following amounts were obtained from the Rietveld analysis, 4% $Zr_{0.5}Ti_{0.5}Cr_{0.5}Ni_{1.5}$, 11% $TiCr_2$ and about 1% $TiCr_{1.5}Ni_{0.5}$.

For the multiphase alloys, a quantitative phase analysis with the Rietveld method has been carried out using the relation [16]:

$$W_p = \frac{S_p(ZMV)_p}{\sum_{i=1}^{n} S_i(ZMV)_i}$$

where W_p is the relative weight fraction of the phase p in a mixture of n phases, S, Z, M and V are, respectively, the Rietveld scale factor, the number of formula units per unit cell, the mass of the formula unit (in atomic mass units) and the unit cell volume (in $Å^3$).

The crystallographic description of the different phases used is reported in Table 1 [17]. During the refinement procedures, some assumptions were adopted: for the hexagonal C14-type structure, a random occupation of the A-site and B-site by Zr–Ti and Cr–Ni atoms respectively. The occupancy of the metallic sites was fixed to the nominal composition. During the Rietveld analysis, we refined the lattice parameters, the atomic positions, the thermal and the peak shape parameters.

The refinement results of the $Zr_{1-y}Ti_y(Cr_{1-x}Ni_x)_2$ series

Table 1
Space group, lattice parameter and atomic positions of the differents phases used in this work taken from reference [17]

Phase	Space group	Lattice parameters		Crystal structure		
$ZrCr_2$ (C14)	$P6_3/mmc$ (194[a])	$a=5.102$ Å	Zr (4f[b])	$x=1/3$	$y=2/3$	$z=0.057$
		$c=8.273$ Å	Cr (2a)	$x=0.0$	$y=0.0$	$z=0.0$
			Cr (6h)	$x=0.829$	$y=0.658$	$z=1/4$
$TiCr_2$ (C14)	$P6_3/mmc$ (194)	$a=4.932$ Å	Ti (4f)	$x=1/3$	$y=2/3$	$z=0.0625$
		$c=8.005$ Å	Cr (2a)	$x=0.0$	$y=0.0$	$z=0.0$
			Cr (6h)	$x=0.833$	$y=0.666$	$z=1/4$
$ZrCr_2$ (C15)	$Fd(3)m$ (227)	$a=7.218$ Å	Zr (8a)	$x=0.0$	$y=0.0$	$z=0.0$
			Cr (16d)	$x=5/8$	$y=5/8$	$z=5/8$
ZrNi	$Cmcm$ (63)	$a=3.268$ Å	Zr (4c)	$x=0$	$y=03609$	$z=1/4$
		b=9.937 Å	Ni (4c)	$x=0$	$y=0.0817$	$z=1/4$
		$c=4.101$ Å				
Zr_9Ni_{11}	$I4/m$ (87)	$a=9.88$ Å	Zr (2a)	$x=0.0$	$y=0.0$	$z=0.0$
		$c=6.61$ Å	Ni (2b)	$x=0.0$	$y=0.0$	$z=1/2$
			Ni (4d)	$x=0.0$	$y=1/2$	$z=1/4$
			Zr (8h)	$x=0.405$	$y=0.210$	$z=0.0$
			Zr (8h)	$x=0.108$	$y=0.305$	$z=0.0$
			Ni (16i)	$x=0.225$	$y=0.125$	$z=0.22$
Zr_7Ni_{10}	$Aba2$ (41)	$a=9.211$ Å	Zr (4a)	$x=0.0$	$y=0.0$	$z=0.9545$
		b=9.156 Å	Zr (4a)	$x=0.0$	$y=0.0$	$z=0.6434$
		$c=12.386$ Å	Zr (4a)	$x=0.0$	$y=0.0$	$z=0.2572$
			Ni (8b)	$x=0.21$	$y=0.0008$	$z=0.7582$
			Ni (8b)	$x=0.2915$	$y=0.0082$	$z=0.5956$
			Ni (8b)	$x=0.0031$	$y=0.2919$	$z=0.5978$
			Ni (8b)	$x=0.0122$	$y=0.2986$	$z=0.3082$
			Ni (8b)	$x=0.1063$	$y=0.109$	$z=0.4501$
			Zr (8b)	$x=0.2459$	$y=0.256$	$z=0.7018$
			Zr (8b)	$x=0.3129$	$y=0.3106$	$z=0.4529$
TiNi	$Pm(-3)m$ (221)	$a=3.007$ Å	Ti (1b)	$x=0.5$	$y=0.5$	$z=0.5$
			Ni (1a)	$x=0.0$	$y=0.0$	$z=0.0$
Cr	$Im(-3)m$ (229)	$a=2.8844$ Å	Cr (2a)	$x=0.0$	$y=0.0$	$z=0.0$
Ni	$Fm(-3)m$ (225)	$a=3.535$ Å	Ni (4a)	$x=0.0$	$y=0.0$	$z=0.0$

[a] Represents the space group number taken from the international crystallographic tables.
[b] The symbols inside the parenthese indicate the Wyckoff notation.

are reported in Table 2. We can note that the reliability indicators used to ascertain the fit quality [18], R_{wp} (weighted profile), and the ''goodness of fit'' S indicate a satisfactory global fit, the S and R_{wp} values are in the range $1.15\% \leq S < 3.13\%$ and $6.76 < R_{wp} < 19.30\%$. For the major phases, the lattice parameters were obtained with high accuracy; the estimated standard deviation (E.S.D.) values are in the range of 10^{-4} Å, while for the others phases, the E.S.D. is about 10^{-3} Å. The atomic positions are also obtained with the same precision as the lattice parameters. Only the thermal parameters were obtained with higher E.S.D..

Because of the large number of alloys investigated in this work, we show in Table 3 the detailed result of the Rietveld analysis for the $Zr_{0.5}Ti_{0.5}Cr_{1.0}Ni_{1.0}$ alloy as an example of a multiphase system. Fig. 1 shows the X-ray powder diffraction pattern fitting by the Rietveld refinement.

3.1.1. Phases stability

From the map of phase relationships for the $Zr_{1-y}Ti_y(Cr_{1-x}Ni_x)_2$ system (Fig. 2) we note a gradual appearance of additional Ni-related phases such as ZrNi–Zr_9Ni_{11}–Zr_7Ni_{10}–TiNi. The precipitation of secondary phases in the quaternary Zr–Ti–Cr–Ni system is strongly dependent on both the Ni and Ti concentrations. With increasing rate of Ni substitution, we noticed the appearance of the ZrNi phase for the composition $ZrCr_{1.5}Ni_{0.5}$, the Zr_9Ni_{11} and Z_7Ni_{10} phases for $ZrCr_{1.0}Ni_{1.0}$ and the Z_7Ni_{10} phase for higher Ni contents. When the Zr is replaced by Ti, for $x_{Ti} \leq 0.5$, only the Ni–Zr phases appeared. For higher Ti contents, the TiNi phase appeared. The amount of Zr_7Ni_{10} phase decreases while the amount of TiNi increases.

With increasing rate of Ni substitution, the amount of the secondary phases increases with the precipitation of pure Cr which is due to the non stability of the $ZrNi_2$ and $TiNi_2$ phases.

We have calculated the heat of formation of the observed secondary phases (ZrNi, Zr_9Ni_{11}, Zr_7Ni_{10} and TiNi) using Miedema's model [19]. The values obtained are reported in Table 4. The values of the heat of formation of the Ni-intermetallic compounds are almost the same. The value of TiNi is quite different. In the $Zr_{1-y}Ti_y(Cr_{1-x}Ni_x)_2$ system and for $x_{Ti} \leq 0.5$, the appear-

Table 2
X-ray Rietveld analysis results of the $Zr_{1-y}Ti_yCr_{2-x}Ni_x$ series

Samples	R_{wp} (%)	S	Phases	Rate (%)	RI (%)	Lattices parameters (Å)
1-$ZrCr_2$	15.05	2.77	C14	52.39	11.75	$a=5.1092(3)$, $c=8.2769(5)$
			C36	47.00	11.21	$a=5.1004(7)$, $c=16.6006(22)$
			ZrN	0.61	8.95	$a=4.6105(0)$
2-$ZrCr_{1.5}$Ni0.5	10.03	1.85	C14	93.60	3.79	$a=5.0494(2)$, $c=8.2763(4)$
			ZrNi	6.40	3.41	$a=3.266(2)$, $b=9.962(7)$, $c=4.104(2)$
3-$ZrCr_{1.0}Ni_{1.0}$	8.57	1.75	C14	58.96	3.08	$a=5.0121(3)$, $c=8.2080(4)$
			C15	29.58	3.67	$a=7.0625(5)$
			Zr_7Ni_{10}	8.20	4.76	$a=9.217(2)$, $b=9.181(2)$, $c=12.349(2)$
			Zr_9Ni_{11}	3.26	3.12	$a=9.878(4)$, $c=6.600(4)$
16-$ZrCr_{0.5}Ni_{1.5}$	10.63	1.94	C15	54.00	3.67	$a=7.0245(2)$
			Zr_7Ni_{10}	42.92	3.44	$a=9.163(1)$, $b=9.133(1)$, $c=12.301(2)$
			Cr	3.08	1.08	$a=2.9035(6)$
4-$Zr_{0.75}Ti_{0.25}Cr_2$	19.13	3.13	C14	97.54	6.32	$a=5.0778(7)$, $c=8.2188(11)$
			Cr	2.46	4.33	$a=2.8867(23)$
5-$Zr_{0.75}Ti_{0.25}Cr_{1.5}Ni_{0.5}$	11.66	2.04	C14	100	3.29	$a=5.0097(4)$, $c=8.2078(7)$
10-$Zr_{0.25}Ti_{0.75}Cr_2$	12.34	1.64	C14	100	4.07	$a=4.9783(3)$, $c=8.0524(4)$
11$Zr_{0.25}Ti_{0.75}Cr_{1.5}Ni_{0.5}$	10.24	1.42	C14	84.24	2.70	$a=4.9310(3)$, $c=8.0655(4)$
			TiNi	6.75	1.59	$a=3.0516(3)$
			Cr	9.01	0.95	$a=2.9157(2)$
12-$Zr_{0.25}Ti_{0.75}Cr_{1.0}Ni_{1.0}$	9.67	1.37	C14	43.62	5.64	$a=4.9103(5)$, $c=8.0176(10)$
			TiNi	42.52	1.84	$a=3.0407(4)$
			Cr	13.86	2.90	$a=2.9070(2)$
13-$TiCr_2$	16.36	1.81	C16	47.12	4.37	$a=4.9133(9)$, $c=15.9821(36)$
			C14	40.30	3.51	$a=4.9169(10)$, $c=7.9746(10)$
			TiCr	10.85	4.65	$a=2.9695(7)$
			Ti	1.74	2.86	$a=3.231(2)$
14-$TiCr_{1.5}Ni_{0.5}$	12.03	1.35	C14	52.81	4.73	$a=4.8836(3)$, $c=7.9781(5)$
			TiNi	20.61	3.02	$a=3.0166(7)$
			TiCr	1.18	0.79	$a=3.0789(14)$
			Cr	25.39	3.15	$a=2.9290(1)$
15-$TiCr_{1.0}Ni_{1.0}$	11.78	1.31	TiNi	74.68	1.79	$a=3.0042(4)$
			Cr	24.49	3.26	$a=2.8990(1)$
			Ti	0.83	2.48	$a=3.2428(19)$
6-$Zr_{0.75}Ti_{0.25}Cr_{1.0}Ni_{1.0}$	11.10	2.00	C14	86.66	2.39	$a=4.9729(4)$, $c=8.1404(6)$
			Zr_7Ni_{10}	11.36	2.73	$a=9.073(6)$, $b=9.036(5)$, $c=12.177(5)$
			Cr	1.98	3.05	$a=2.8603(10)$
18-$Zr_{0.75}Ti_{0.25}Cr_{0.5}Ni_{1.5}$	10.63	2.07	C15	65.53	3.41	$a=6.9778(2)$
			Zr_7Ni_{10}	29.42	3.63	$a=9.052(2)$, $b=9.027(3)$, $c=12.179(2)$
			Zr_9Ni_{11}	2.78	4.18	$a=9.829(12)$, $c=6.669(7)$
			Cr	2.26	2.39	$a=2.9012(4)$
7-$Zr_{0.50}Ti_{0.50}Cr_2$	14.31	1.99	C14	100	4.43	$a=5.0216(8)$, $c=8.1333(12)$
8-$Zr_{0.50}Ti_{0.50}Cr_{1.5}Ni_{0.5}$	10.94	1.71	C14	100	2.69	$a=4.9708(3)$, $c=8.1403(6)$
9-$Zr_{0.50}Ti_{0.50}Cr_{1.0}Ni_{1.0}$	6.76	1.15	C14	55.03	0.82	$a=4.9525(3)$, $c=8.0933(5)$
			Zr_7Ni_{10}	16.43	1.35	$a=9.016(7)$, $b=8.980(7)$, $c=12.125(7)$
			TiNi	17.99	0.80	$a=3.067(2)$
			Cr	10.55	0.64	$a=2.8996(3)$
20-$Zr_{0.50}Ti_{0.50}Cr_{0.5}Ni_{1.5}$	16.11	2.41	C15	38.32	6.61	$a=6.9338(4)$
			Zr_7Ni_{10}	41.42	6.56	$a=8.978(3)$, $b=8.941(3)$, $c=12.085(3)$
			TiCr	3.85	5.59	$a=2.926(0)$
			Cr	8.02	9.19	$a=2.8936(3)$
			TiNi	5.61	5.54	$a=2.9812(8)$
			Ti	2.77	3.03	$a=2.996(6)$, $b=4.488(15)$

ance of the Ni–Zr phases can be related to the nominal Ni concentrations. For higher Ti substitutions, the Ti content controls the appearance of the additional phases.

3.1.2. The hexagonal C14-type structure

In Fig. 3, we plotted the evolution of the cell volume for the hexagonal C14-type structure versus Ti content for the different Ni concentrations ($x_{Ni}=0.0$, $x_{Ni}=0.5$, $x_{Ni}=1.0$). We can notice a decrease of the cell volume with increasing Ti content along a straight line which is in good agreement with the atomic radius reduction occurring on the Zr(Ti) site ($r_{Ti}=1.462$ Å$<r_{Zr}=1.602$ Å [20]). The lines are shifted depending on the Ni content. On the other hand, a decrease of the cell volume with Ni content is due

Table 3
Crystal structure refinements results for the $Zr_{0.5}Ti_{0.5}Cr_{1.0}Ni_{1.0}$ alloy (the values in parentheses represent the estimated standard deviation for the last digit)

Phase	Space group	Lattice parameters	Coordinates (x, y, z)	Thermal parameter
$Zr_{0.5}Ti_{0.5}Cr_{1.0}Ni_{1.0}$	*P63/mmc* (194)	$a=4.9525(3)$ Å	z(Zr)=0.0623(4)	B(Zr)=0.09(12) Å^2
		$c=8.0933(5)$ Å	x(Cr2)=0.8297(9)	B(Cr1)=0.07(20) Å^2
				B(Cr2)=0.63(14) Å^2
Zr_7Ni_{10}	*Aba2* (41)	$a=9.016(7)$ Å	z(Zr1)=0.964(8)	B(Zr)=1.9(8) Å^2
		$b=8.980(7)$ Å	z(Zr2)=0.638(5)	
		$c=12.125(7)$ Å	z(Zr4)=0.725(6)	
			z(Zr5)=0.453 (8)	
			z(Ni1)=0.827(10)	B(Ni)=0.4(10) Å^2
			z(Ni2)=0.598(18)	
			z(Ni3)=0.602(15)	
			z(Ni5)=0.425(8)	
TiNi	*Pm(−3)m* (221)	$a=3.067(2)$ Å		B(Ti)=3(1) Å^2
				B(Ni)=5(2) Å^2
Cr	*Im(−3)m* (229)	$a=2.8996(3)$ Å		B(Cr)=0.2 Å^2

to the reduction of the Cr(Ni) site size ($r_{Ni}=1.246$ Å$<r_{Cr}=1.282$ Å [20]). This phenomenon can be explained by a change in the atomic bond distance [21].

For the compounds containing 25% of Ni (Fig. 3), the replacement of Zr by Ti the system is single phase only for the first two Ti concentrations ($y=0.25$ and 0.5). For Ti contents higher than 0.5, the system becomes multiphase with the appearance of the TiNi phase and pure Cr. It seems that in the $TiCr_2$ compound, the replacement of Cr by Ni is probably not effective or limited to a critical amount due to the non stability of the $TiNi_2$ compound [14]. No study has been reported on this subject.

From Fig. 3, we can see that the unit cell volume of $TiCr_{1.5}Ni_{0.5}$ is smaller than that of $TiCr_2$, the corresponding volume reduction is about 2.3%. The change in the unit cell volume relative to the parent compound $TiCr_2$ for the compound with the nominal composition $TiCr_{1.5}Ni_{0.5}$ can be caused by:

i) a real substitution of the Ni atoms on the Cr metallic sites,

ii) as the phase abundance of the as-cast alloy $TiCr_{1.5}Ni_{0.5}$ shows the appearance of the secondary phase TiNi and the precipitation of pure Cr (20.6% and 25.4% respectively), the formation of off-stoichiometry $Ti_{1+x}Cr_{2-x}$ is also possible as has been found in the $TiMn_2$ system and confirmed by a neutron diffraction study of $Ti_{1.2}Mn_{1.8}$ [22].

The second assumption can be excluded for the simple reason that off-stoichiometric $Ti_{1+x}Cr_{2-x}$ if it would exist leads to an increase of the cell volume ($r_{Ti}=1.40$ Å$>r_{Cr}=1.282$ Å). Hence, we can confidently retain the first hypothesis. The replacement of some Cr by Ni atoms is

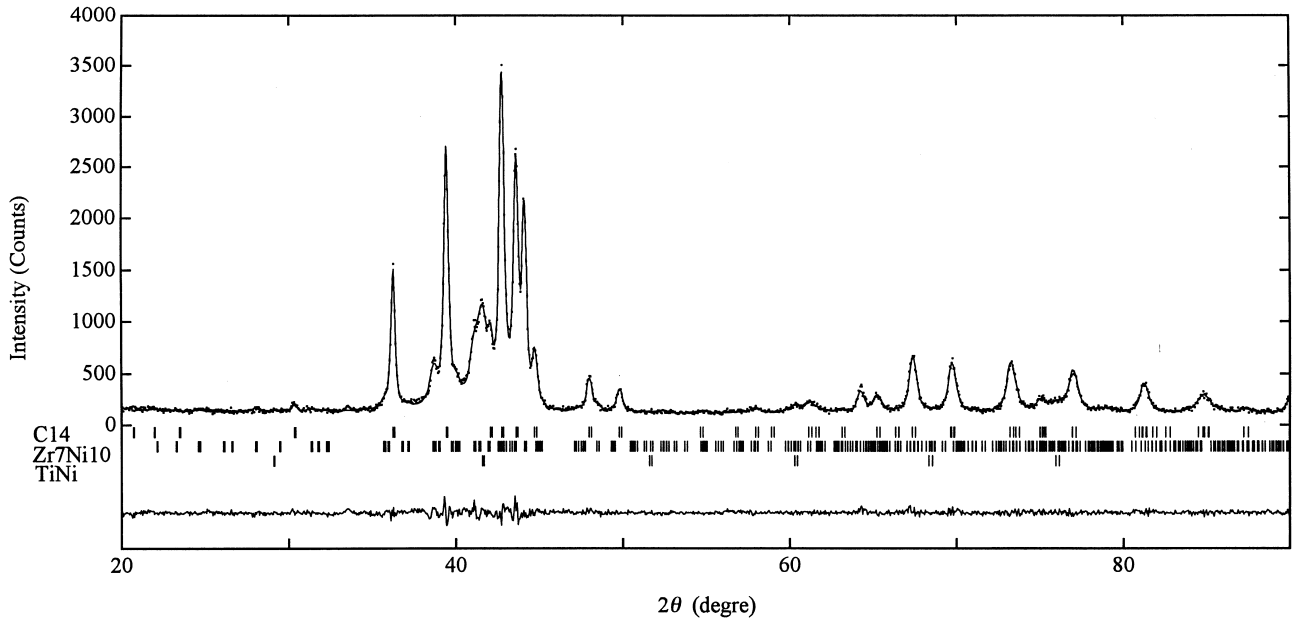

Fig. 1. X-ray Rietveld analysis of the $Zr_{0.5}Ti_{0.5}(Cr_{0.5}Ni_{0.5})_2$ as-cast alloy (dots: experimental intensity, upper solid line: calculated intensity, lower solid line: the intensity difference, vertical bars represent the Bragg diffraction peaks of phases).

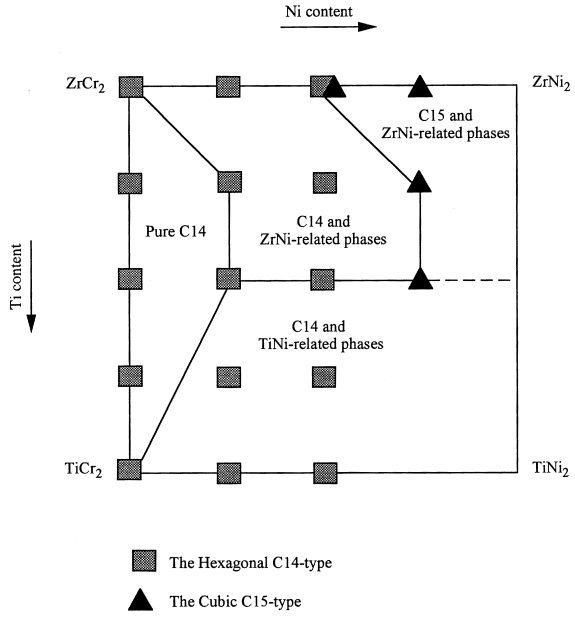

Fig. 2. Map of phase relationships in the $Zr_{1-y}Ti_y(Cr_{1-xNix})_2$ system obtained from the quantitative phase analysis using the Rietveld method.

quite possible as it contributes to the decrease of the cell volume because of the radius reduction ($r_{Ni}=1.246$ Å$<r_{Cr}=1.282$ Å).

Since the X-ray scattering length of the Cr and Ni are very similar ($\Delta z/z=0.167$), we are unable to refine the occupancy of the 2a and 6h metallic sites from the X-ray data in order to confirm the substitution of the Ni on the Cr site. In the case of the neutron diffraction however, the two elements can easily be distinguished, the scattering length [23] of the two elements being quite different ($\Delta b/b=1.834$).

3.1.3. The Zr_7Ni_{10} phase

The Zr_7Ni_{10} phase has been found to appear for higher Ni concentrations and it's amount increases with increasing Ni-substitution. In the pseudo-binary $Zr(Cr_{1-x}Ni_x)_2$ system, the lattice parameters of the orthorhombic phase Zr_7Ni_{10} do not seem to be affected by the nominal composition. In the previous work of Joubert et al. [11], for the several compositions studied, we can notice that the Zr_7Ni_{10} phase keeps almost the same unit cell volume. In this study, the replacement of Zr by Ti seems to have some influence on the Zr_7Ni_{10} phase. The refined lattice parameters obtained from the X-ray Rietveld analysis show some difference compared to the values reported in Table 2. Fig. 4 presents the evolution of the Zr_7Ni_{10} unit cell volume versus Ti content for 75% Ni substitution. We can see clearly a decrease of the unit cell volume with the replacement of Zr by Ti. The stability of the Zr_7Ni_{10} phase with lower unit cell volume than that of the stoichiometric binary composition is interesting from the point of view of the crystal structure and thermodynamic properties. In the Ti–Ni phase diagram [14], no phase similar to Zr_7Ni_{10} (like Ti_7Ni_{10}) has been reported. From our results, we can attribute the decrease of the cell volume to the replacement of Zr by Ti, a replacement of Ni by Cr being excluded because it would lead to an increase of the cell volume.

Table 4
Heat of formation of the ZrNi, Zr_9Ni_{11}, Zr_7Ni_{10} and TiNi compounds calculated using Miedema's model [19]

Compounds	Ni content	ΔH (kJ g^{-1} atom^{-1} of alloy)	$\Delta H/x_{Ni}$ (kJ g^{-1} atom^{-1} of Ni)
ZrNi	50%	−42.08	−84.16
Zr_9Ni_{11}	55%	−42.63	−77.51
Zr_7Ni_{10}	59%	−42.63	−73.5
TiNi	50%	−33.15	−66.30

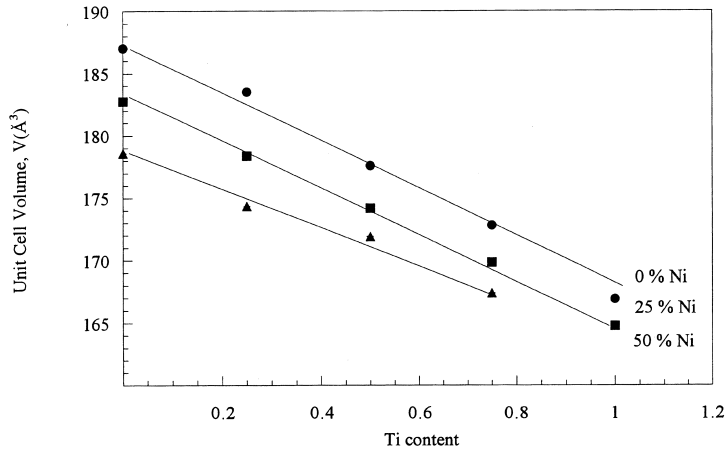

Fig. 3. Evolution of the unit cell volume of the hexagonal Laves phase type-structure (C14) versus the Ti and Ni concentrations.

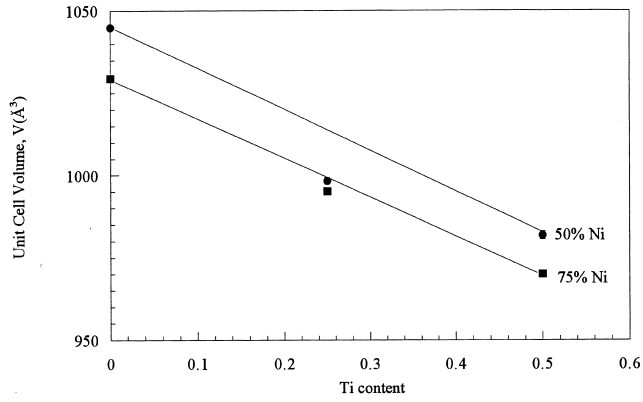

Fig. 4. Evolution of the unit cell volume of the orthorhombic Zr_7Ni_{10} phase versus the Ti content.

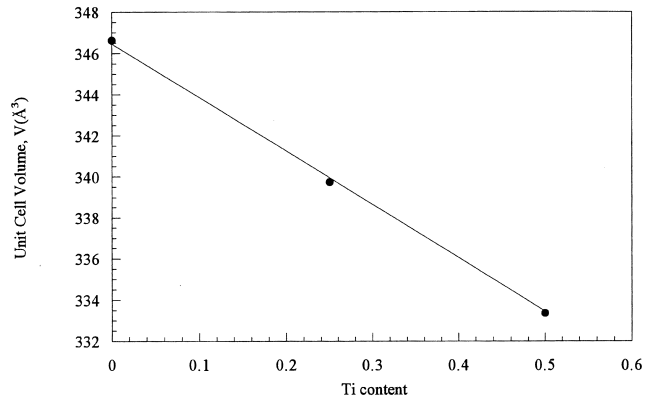

Fig. 5. Evolution of the unit cell volume of the cubic Laves phase type-structure (C15) versus the Ti content.

The P–C–T measurements on the $Zr_7Ni_{10}H_{14}$ (1.13 wt.%) phase show a relatively low and flat plateau pressure, $P_{eq}=0.04$ bars at 298 K [24,25]. However, if a replacement of Zr by Ti occurs, the thermodynamic properties will be modified and in particular the plateau pressure. According to the empirical correlation between the plateau pressure and the cell volume already obtained for other hydrogen absorbing pseudo-binary systems such as $La(Ni_{1-x}M_x)_5$ [26] and $Zr(Mn_{1-x}M_x)_2$ [27], the replacement of Zr by Ti in the Zr_7Ni_{10} compound will increase the plateau pressure. In Table 5, we have reported the rate of change in the cell volume accompanying the formation of the major phases of the $Zr_{1-y}Ti_y(Cr_{1-x}Ni_x)_2$ series (the hexagonal C14, the cubic C15 and the Zr_7Ni_{10} phase). We can see that the change of the unit cell volume for the Zr_7Ni_{10} phase is significant compared to the C14 and C15 Laves phases.

3.1.4. The cubic C15-type structure

A crystal structure change from the hexagonal C14-type to the cubic C15-type in the $Zr_{1-y}Ti_y(Cr_{1-x}Ni_x)_2$ pseudo-binary system is found at higher Ni content ($x_{Ni}>1.0$) and independent of the replacement of Zr by Ti. Only for the composition $ZrCr_{1.0}Ni_{1.0}$, we found both Laves phases with 60% of C14 and 30% of C15. As found for the hexagonal phase, the unit cell volume of the cubic phase decreases with increasing the Ti content (Fig. 5).

3.2. Thermodynamic properties

3.2.1. Variation of the heat of formation with composition

The replacements on both metallic sites, Zr by Ti and Cr by Ni, results in a decrease of unit cell volume because of the change of the metallic site radii with respect to those of the parent compound $ZrCr_2$. But the rate of this reduction increases with increasing Ti substitution, being about three times that of the Ni substitution. Therefore, in our systematic investigation of the $Zr_{1-y}Ti_y(Cr_{1-x}Ni_x)_2$ system, the Ti concentration step was taken smaller than for Ni, to allow for a better control of the unit cell volume change.

The semi-empirical model based on the electronic structure of the host metal developed by Griessen et al. [28] has shown values in good agreement with experiments. For our $Zr_{1-y}Ti_y(Cr_{1-x}Ni_x)_2$ series, this model was used to estimate the heat of formation of the corresponding hydrides. The heat of formation of the pseudo-binary hydrides $Zr_{1-y}Ti_y(Cr_{1-x}Ni_x)_2H_x$ can be considered a linear summation of that of the ternary hydrides:

$$\begin{aligned}\Delta H(Zr_{1-y}Ti_yCr_{2-x}Ni_xH_m) &= (1 - x/2)\,\Delta H(Zr_{1-y}Ti_yCr_2H_m) \\ &\quad + (x/2)\Delta H(Zr_{1-y}Ti_yNi_2H_m) \\ &= (1-x/2)[(1-y)\,\Delta H(ZrCr_2H_m)\end{aligned}$$

Table 5
Rate of the change in the unit cell volume for the hexagonal and cubic Laves phase and the orthorhombic Zr_7Ni_{10} phase with the Ti content (in %)

Ti content	C14			C15	Zr_7Ni_{10}
	$x_{Ni}=0.0$	$x_{Ni}=0.25$	$x_{Ni}=0.5$		
0.0	−0.0	−2.29	−4.52	−7.85	−1.44
0.25	−1.87	−4.61	−6.78	−9.60	−4.84
0.50	−5.03	−6.86	−8.08	−11.72	−7.75

Table 6
Heat of formation of the $ZrCr_2H_m$, $TiCr_2H_m$, $ZrNi_2H_m$ and $TiNi_2H_m$ hydrides calculated from the band structure model [23] and used for the estimation of the heat of formation of the pseudo-binaries $Zr_{1-y}Ti_yCr_{2-x}Ni_xH_{2m}$ hydrides series

Hydrides	$\Delta H_{B.S.M.}$ (kJ mol^{-1} H)
$ZrCr_2H_m$	−33.2
$ZrNi_2H_m$	−19.0
$TiCr_2H_m$	−32.9
$TiNi_2H_m$	−3.50

$$+ (y)\ \Delta H(TiCr_2H_m)]$$
$$+ (x/2)[(1$$
$$- y)\ \Delta H(ZrNi_2H_m)$$
$$+ (y)\ \Delta H(TiNi_2H_m)]$$

Where $\Delta H(AB_2H_m)$ represents the heat of formation of the ternary hydrides. The values are listed in Table 6 in which x and y represent the nominal nickel and titanium concentrations, respectively and m the hydrogen content. In Fig. 6, we have plotted the variation of the calculated heat of formation of the $Zr_{1-y}Ti_y(Cr_{1-x}Ni_x)_2H_x$ hydrides versus Ti content for the different Ni concentrations. The heat of formation of the pseudo-binary $Zr_{1-y}Ti_y(Cr_{1-x}Ni_x)_2H_x$ system decreases with increasing substitution of both Ti and Ni, the $Zr_{1-y}Ti_y(Cr_{1-x}Ni_x)_2H_x$ hydrides are less stable than the parent hydride $ZrCr_2H_{3.4}$.

An empirical correlation between the plateau pressure and the unit cell volume of the alloys for $LaNi_5$ [26] and $ZrMn_2$ [27] systems has been already reported. In this study, we would like to show the evolution of the calculated heat of formation and the alloy volumes determined by X-ray Rietveld analysis. The heat of formation of the hydrides can be found through the Van't Hoff rule:

$$RT\ln P = \Delta H - T\ \Delta S$$

where ΔH represents the heat of formation, ΔS the entropy, T the temperature, P the plateau pressure and R the gas constant.

From Fig. 7, a good linear fit was obtained indicating the correlation between the plateau pressure and the $Zr_{1-y}Ti_y(Cr_{1-x}Ni_x)_2$ unit cell volume.

3.2.2. Pressure–composition isotherms

We have selected some alloys from the $Zr_{1-y}Ti_y(Cr_{1-x}Ni_x)_2$ series and measured the isotherm at 313 K and for the $Zr_{0.5}Ti_{0.5}Cr_{1.5}Ni_{0.5}$ alloy an isotherm at 373 K has been measured. The absorption–desorption curves are reported in Fig. 8.

During the P–C–T measurements, the single phase samples $Zr_{0.75}Ti_{0.25}Cr_{1.5}Ni_{0.5}$ and $Zr_{0.5}Ti_{0.5}Cr_{1.5}Ni_{0.5}$ showed very poor kinetics and, therefore, P–C–T isotherms can not be measured correctly. The alloys shows relatively better kinetics at 373 K but these are still not good enough to measure P–C–T isotherm.

On the contrary, in the multiphase samples, kinetics were strongly enhanced in comparison to the single phase systems. The isotherms can be easily measured. The multiphase system seems to behave as single phase, their PCT curves present a single plateau with a slope.

From Fig. 8, we can notice that the two corresponding hydrides $Zr_{0.75}Ti_{0.25}Cr_{1.0}Ni_{1.0}H_{2.94}$ and $Zr_{0.25}Ti_{0.75}Cr_{1.5}Ni_{0.5}H_{2.31}$ can not be completely dehydrogenated, the desorption curves did not return to $H/M = 0.0$, $H/M = 0.19$ (0.30 wt.%) and 0.22 (0.40 wt.%) for the two compositions, respectively. From the quantitative phase analysis, we know that the two alloys contain the hexagonal C14-type as major phase with 11% of the Zr_7Ni_{10} phase with 2% of Cr for the the $Zr_{0.75}Ti_{0.25}Cr_{1.0}Ni_{1.0}$ alloy, and 7% of the TiNi phase with 9% Cr for the $Zr_{0.25}Ti_{0.75}Cr_{1.5}Ni_{0.5}$ alloy. We think that the reduction of the reversible hydrogen capacity can be attributed to the nature of the secondary phases and their relative amount.

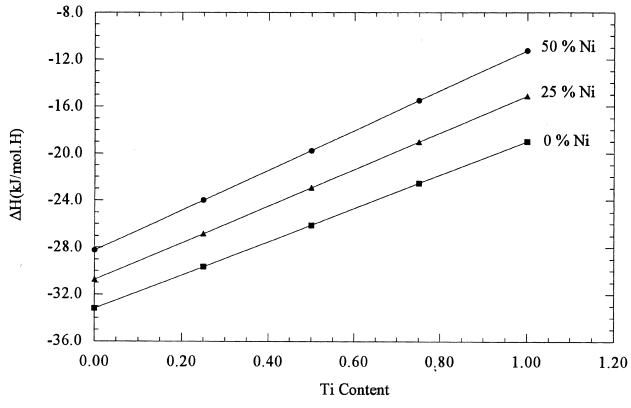

Fig. 6. Variation of the calculated heat of formation of the $Zr_{1-y}Ti_y(Cr_{1-xNix})_2H_m$ hydrides with the Ti and Ni concentrations.

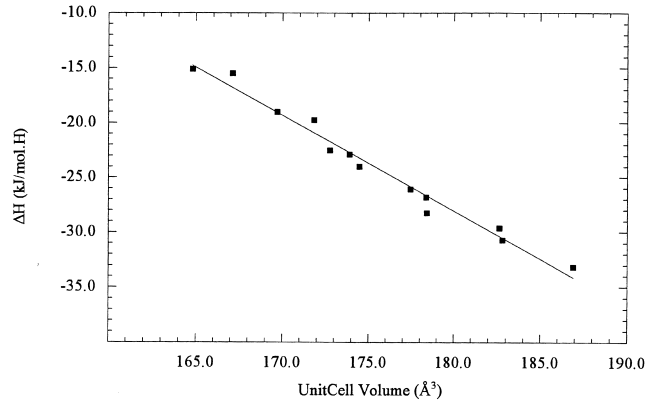

Fig. 7. Variation of the calculated heat of formation of the $Zr_{1-y}Ti_y(Cr_{1-x}Ni_x)_2H_m$ hydrides versus the experimental unit cell volume determined by the Rietveld analysis.

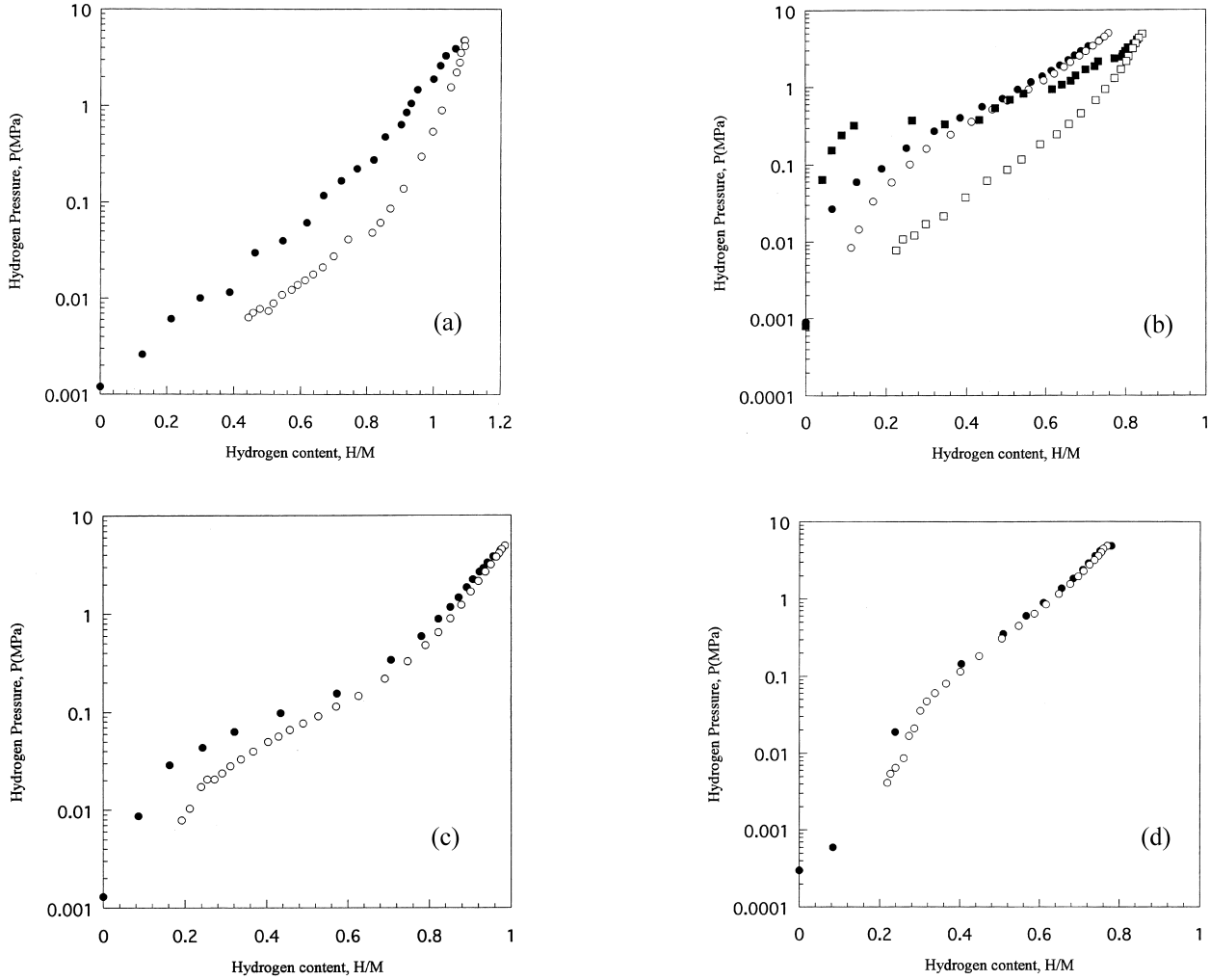

Fig. 8. Pressure–composition isotherm measured at 313 K for (a) $Zr_{0.75}Ti_{0.25}(Cr_{0.75}Ni_{0.25})_2$ (b) $Zr_{0.5}Ti_{0.5}(Cr_{0.75}Ni_{0.25})_2$ (c) $Zr_{0.75}Ti_{0.25}(Cr_{0.5}Ni_{0.5})_2$ and (d) $Zr_{0.25}Ti_{0.75}(Cr_{0.75}Ni_{0.25})_2$ (the filled symbols represent the absorption curve and the empty symbols for the desorption curve).

The plateaus of the measured samples present a relatively steep slope. The origin of the plateau slope in the Laves phases can be due to the segregation phenomenon, the X-ray diffraction pattern shows rather broad peaks or a multiple sub-peaks, the Bragg peaks being wider than for well-crystallized samples. Sandrock reported that a heat treatment before the activation reduced the slope [29].

As seen in Fig. 8, the $Zr_{0.75}Ti_{0.25}Cr_{1.0}Ni_{1.0}$ alloy, despite its strong plateau slope, shows almost no hysteresis. For the $Zr_{0.25}Ti_{0.75}Cr_{1.5}Ni_{0.5}$ alloy, the hysteresis is seen in Fig. 8 to more pronounced at lower pressures. The hysteresis phenomenon can be attributed for a large part to the alloy composition, i.e, the Zr/Ti ratio on the 4f metallic site and the Cr/Ni ratio on the 2a and 6h metallic sites.

The selected alloys absorb a large amount of hydrogen, $H/M \geq 1.4$ wt.% (Table 7). We note that the two alloy compositions leading to a single hexagonal phase have higher capacity but unfortunately, the hydrogen absorbed can not be completely desorbed. The origin of the partial

Table 7
Hydrogen capacity and theoretical discharge capacity for the selected alloys

Alloy	H/M (H/f.u.)	H/M (wt.%)	P (MPa)	C_{th} [a] (mA h g^{-1})
$Zr_{0.75}Ti_{0.25}Cr_{1.5}Ni_{0.5}$	1.09	1.75	4.706	467
$Zr_{0.75}Ti_{0.25}Cr1.0Ni_{1.0}$	0.98	1.56	4.902	417
$Zr_{0.5}Ti_{0.5}Cr_{1.5}Ni_{0.5}$	0.84	1.44	4.923	387
$Zr_{0.25}Ti_{0.75}Cr_{1.5}Ni_{0.5}$	0.77	1.40	4.860	372

[a] $C_{th}=(F\times[H/M])/(3.6\times M_{av})$ represent the theoretical discharge capacity where F(9.6487 104 C mol.−1) is the Faraday constant, H/M the hydrogen capacity and M is the average atomic weight of the alloy [31].

reversibility of the hydrogen uptake is mainly due to their poor kinetics. It is very important to know that by changing the alloy composition of the parent compound $ZrCr_2$ by substitutions on both metallic sites (Zr/Ti and Cr/Ni), we can conserve a large hydrogen capacity along with a strong modification of the thermodynamic properties, in particular the plateau pressure. The hydrides of the selected compositions are less stables than $ZrCr_2H_{3.4}$, which present a very low plateau pressure ($P=12$ kPa at 293 K).

4. Discussion

From the Rietveld analysis, the investigation of the pseudo-binary $Zr_{1-y}Ti_y(Ni_{1-x}Cr_x)_2$ series shows that the alloys are generally obtained as multiphase systems. The map of phase relationships of the system depends strongly on the nominal composition. The appearance of the additional phases was found to be correlated with the Ni content for the lower Ti concentrations ($y_{Ti}<0.5$). For the higher Ti contents, the Ti–Ni phases became more stable than the Zr–Ni phases. The crystal structure change from the hexagonal phase to the cubic one occurs at higher Ni concentrations ($x_{Ni}>0.5$). At higher Ti concentrations ($y_{Ti}>0.5$), the cubic phase can be stabilized but the amount is smaller. The instability of the cubic phase for $x_{Ni}>0.5$ and $y_{Ti}>0.5$ can be due to the non existence of both the $ZrNi_2$ and the $TiNi_2$ compound. The system has a tendency to crystallize in the Ni–Zr or Ni–Ti phases due to Ni and Ti high concentrations. The lattice parameters of the major phases, C14 and C15 phases were found to be well correlated with the nominal Ti and Ni concentrations.

Lei et al. [30], in their study of the system $Zr(Ni_{1-x}Cr_x)_2$ with $0.15\leq x\leq 0.65$, reported a structural transition. The hexagonal C14-type changed to the cubic C15-type in the composition range $x=0.45-0.50$. For higher nickel content ($x_{Ni}>0.5$), the authors observed the formation of the secondary Zr_7Ni_{10} phase. The alloys with $x_{Ni}=0.65$ show a good electrochemical discharge capacity (a discharge capacity of about $c=305$ mA h g^{-1} at ambient temperature was found for the compound $ZrCr_{0.7}Ni_{1.3}$) and have long electrochemical charge–discharge cycle lives.

In their study of the Zr–Cr–Ni ternary phase diagram at 1273 K, Joubert et al. [11], showed the existence of both C14 and C15 Laves phases with additional Zr–Ni phases. The phase abundance is strongly dependent on the nickel content. The alloy mixture containing both the Laves phase and the Zr–Ni phase shows a considerable enhancement of the electrochemical properties compared to each phase taken independently. On the other hand, a single phase system shows poor electrochemical properties, only about 6.25% of the hydrogen capacity determined by solid–gas measurement can be obtained. The highest discharge capacity at 20 mA h g^{-1} current for the system Zr–Cr–Ni was obtained with the formula $Zr_{33.5}Cr_{24}Ni_{42.5}$, $c=263$ mA h g^{-1}, the sample containing 85% C14 and 15% Zr_7Ni_{10}.

From our results, it seems that the alloy microstructure can play an important role in controlling the hydriding–dehydriding kinetics in Zr-Laves phases. To enhance kinetics, we found that the alloys studied should have at least one second phase. Of course, the problem of poor kinetics can be solved by other methods such as surface treatments or addition of some active rare earth. By changing the alloy composition, we not only improve the kinetics, but we also introduce some modifications of the thermodynamic properties such as the plateau pressure, hysteresis and plateau slope. The change of the thermodynamic properties depend on both the nature and the quantity of the secondary phase.

In Table 7, we report the maximum hydrogen capacity determined from the P–C–T diagrams and the corresponding calculated discharge capacity. We note that the measured samples showed a relatively high discharge capacity. Further investigation of the electrochemical properties of the $Zr_{1-y}Ti_y(Cr_{1-x}Ni_x)_2$ pseudo-binary system will give more information about the reactivity of the system in alkaline solution (maximum discharge capacity, the cycle life).

5. Conclusion

In the present study, we presented the investigation of the pseudo-binary multiphase system $Zr_{1-y}Ti_y(Cr_{1-x}Ni_x)_2$. By means of X-ray Rietveld analysis, we have been able to determine the phase map within the selected compositions. From the results, we conclude that:

– a linear relationship between the lattice parameters and the (Ti, Ni) contents has been obtained for both the hexagonal and cubic Laves phases,
– the cell volume of the Zr_7Ni_{10} has been found to vary with the Ti composition. The variation of the volume versus the Ti content shows a decrease of the volume with increasing the Ti concentration in the general formula $Zr_{1-y}Ti_y(Cr_{1-x}Ni_x)_2$. The result indicates a possible substitution of Zr by Ti in the Zr_7Ni_{10} phase.

The measured absorption–desorption isotherms, shows the influence of the nominal composition on the hydrogen uptake, the plateau pressure, the plateau slope, the hysteresis and the kinetics. We found that single phase systems absorb a large hydrogen amount but the kinetics were very poor. On the contrary, multiphase systems have a relatively high hydrogen capacity and the hydrogen absorption–desorption occurs with better kinetics. The systems react as single phase but the PCT curves show a relatively steep plateau slope.

Acknowledgements

One of the authors was an STA fellow and wishes to thank the Science and Technology Agency of Japan for its financial support. We are grateful to Dr. P. Tessier for the reading and his comments on this article.

References

[1] A. Pebler, E.A. Gulbransen, Electrochem. Technol. 4 (1966) 211.
[2] D. Shaltiel, I. Jacob, D. Davidov, J. Less-Common Metals 53 (1977) 117.
[3] P. Nash, C.S. Jayanth, in: T.B. Massalski (Ed.), Binary Alloys Phase Diagrams, 2nd ed., CD-ROM, ASM International, 1996.
[4] A. Drasner, Z. Blazina, J. Alloys Comp. 175 (1991) 103.
[5] A. Drasner, Z. Blazina, J. Alloys Comp. 199 (1993) 101.
[6] I. Jacob, D. Shaltiel, in: T.N. Veziroglu, W. Seifritz (Eds.), Hydrogen Energy Systems, Pergamon, Oxford, 1979, p. 1689.
[7] A. Drasner, Z. Blazina, J. Alloys Comp. 163 (1990) 151.
[8] M. Bououdina, PhD Thesis, Joseph Fourier University, Grenoble, June 1995.
[9] M. Bououdina, J.L. Soubeyroux, D. Fruchart, P. De Rango, J. Alloys Comp. 257 (1997) 82.
[10] J.-M. Joubert, M. Latroche, A. Percheron-Guegan, J. Bouet, J. Alloys Comp. 240 (1996) 219.
[11] J.-M. Joubert, M. Latroche, A. Percheron-Guegan, F. Bouree-Vigneron, J. Alloys Comp. 217 (1995) 283.
[12] F. Izumi, in: R.A. Young (Ed.), The Rietveld Method, Oxford University Press, Oxford, 1993, chapter 13.
[13] K. Nomura, H. Uruno, S. Ono, H. Shinozuka, S. Suda, J. Alloys Comp. 107 (1985) 221.
[14] J.L. Murray, in: T.B. Massalski (Ed.), Binary Alloys Phase Diagrams, 2nd ed., CD-ROM,, ASM International, 1996.
[15] Z.H. Yan, T. Klassen, C. Michaelsen, M. Oehring, R. Bormann, Phys. Rev. B 47(14) (1993) 8520.
[16] R.J. Hill, in: R.A. Young (Ed.), The Rietveld Method, Oxford University Press, Oxford, 1993, chapter 5.
[17] P. Villars, L.D. Calvert, Pearson's Handbook of Crystallographic Data for Intermetallic Phases, 2nd ed., ASM International, 1991.
[18] R.A. Young, in: R.A. Young edition, The Rietveld Method, Oxford University Press, Oxford, 1993, Chapter 1.
[19] A.R. Miedema, R. Boom, F.R. De Boer, Less-Common Metals. 41 (1975) 283.
[20] E. Teatum, K. Gschneidher, J. Waber, Compilation of calculated data useful in predicting metallurgical behaviour of the elements in binary alloy systems, LA-2345, Los Alamos Scientific Laboratory, 1960.
[21] J. Huot, E. Akiba, H. Iba, J. Alloys Comp. 228 (1995) 181.
[22] D. Fruchart, J.L. Soubeyroux, R. Hemplemann, J. Alloys Comp. 99 (1984) 307.
[23] W.B. Yellon, in: F. Grandjean, G.J. Long, K.H.J. Buschow (Eds.), Interstitial Intermetallic Alloys, Nato Asi Series, Series E Applied Sciences, vol. 281, 1995, chapter 9.
[24] F.H.M. Spit, J.W. Drijver, S. Radelaar, Scr. Metall. 14 (1980) 1071.
[25] J.-M. Joubert, M. Latroche, A. Percheron-Guegan, J. Alloys Comp. 231 (1995) 494.
[26] A. Percheron Guegan, in: F. Grandjean, G.J. Long, K.H.J. Buschow (Eds.), Interstitial Intermetallic alloys, Nato Asi Series, Series E Applied Sciences, vol. 281, 1995, chapter 5.
[27] S. Fujitani, I. Yonezu, T. Saoto, N. Furukawa, E. Akiba, H. Hayakawa, S. Ono, J. Alloys Comp. 172–174 (1991) 220.
[28] R. Griessen, T. Riesterer, in: L. Schlapbach (Ed.), Hydrogen In Intermetallic Compounds I, Topics in Applied Physics series, vol. 63, 1988, chapter 6.
[29] G.D. Sandrock, International Hydrogen Energy Systems, 1978, p. 1625.
[30] L. Yongquan, Y. Xiaoguang, W. Jing, W. Qidong, J. Alloys Comp. 231 (1995) 573.
[31] J. Huot, E. Akiba, T. Oguro, Y. Ishido, J. Alloys Comp. 218 (1995) 101.